# Fretting Wear of Ti-48Al-2Cr-2Nb

Kazuhisa Miyoshi,* Bradley A. Lerch, and Susan L. Draper

National Aeronautics and Space Administration

Glenn Research Center

21000 Brookpark Road

Cleveland, Ohio 44135 USA

**Abstract**

An investigation was conducted to examine the wear behavior of gamma titanium aluminide (Ti-48Al-2Cr-2Nb in atomic percent) in contact with a typical nickel-base superalloy under repeated microscopic vibratory motion in air at temperatures from 296 to 823 K. The surface damage observed on the interacting surfaces of both Ti-48Al-2Cr-2Nb and superalloy consisted of fracture pits, oxides, metallic debris, scratches, craters, plastic deformation, and cracks. The Ti-48Al-2Cr-2Nb transferred to the superalloy at all fretting conditions and caused scuffing or galling. The increasing rate of oxidation at elevated temperatures led to a drop in Ti-48Al-2Cr-2Nb wear at 473 K. Mild oxidative wear was observed at 473 K. However, fretting wear increased as the temperature was increased from 473 to 823 K. At 723 and 823 K, oxide disruption generated cracks, loose wear debris, and pits on the Ti-48Al-2Cr-2Nb wear surface. Ti-48Al-2Cr-2Nb wear generally decreased with increasing fretting frequency. Both increasing slip amplitude and increasing load tended to produce more metallic wear debris, causing severe abrasive wear in the contacting metals.

**Keywords**: Titanium aluminide (γ-TiAl), fretting wear, fatigue, oxidation, high temperature

---

* Telephone: 216–433–6078; Facsimile: 216–433–5544; *E-mail address*: miyoshi@grc.nasa.gov

## 1. Introduction

Microscopically small surface-parallel relative motion, which can be vibratory or creeping, produces fresh, clean interacting surfaces and causes adhesion and junction (contact area) growth in the contact zone [1–3]. The interfacial adhesive bonds of the interacting surfaces were generally stronger than the cohesive bonds in a cohesively weaker metal. As a result of the displacement, adhering metal particles are produced so that fretting wear produced between the contacting elements is adhesive wear taking place in a nominally static contact under normal load and repeated microscopic vibratory motion [4–8]. Progressive fretting produces galling. The metal wear particles can oxidize. These oxidized particles are abrasive, subsequently causing abrasive wear (a severe form of wear) of the surfaces. The failure probability of engine components abruptly increases at this stage. Galling and/or abrasive wear in turn can cause premature fatigue-crack initiation. Propagation of such cracks under cyclic loads may result in the failure of the component (blade or disk) and convey fragments into the engine with catastrophic results.

Fretting fatigue is a very complex problem of significant interest to aircraft engine manufacturers [9–12]. Fretting failure can occur in a variety of aircraft engine components, such as low-pressure turbine blades and disks [13–14]. The most damaging effect of fretting is the possible significant reduction in fatigue capability of the fretted component [8]. It was reported that the reduction in fatigue strength of Ti-47Al-2Nb-2Mn with 0.8 vol. % $TiB_2$ by fretting was around 20%.

Fretting failure can occur to a variety of engine components. Numerous approaches have been taken to address the fretting problem depending on the component and operating conditions. The component of interest in this investigation is the fan and compressor blades. Many existing fan and compressor components have titanium alloy disks and airfoils. A concern for these airfoils is the fretting in fit interfaces at the dovetail. Careful design can reduce fretting in most cases but not completely eliminate it, because the airfoils frequently have a skewed (angled) blade-disk dovetail attachment, which leads to a very complex stress state. Further, the local stress state becomes more complicated when the influence of metal-metal contact and the edge of contact is evaluated.

The material of interest in this study is gamma titanium aluminide (γ-TiAl). This material has potential applications for low-pressure turbine blades. A concern for the γ-TiAl blades is fretting at the dovetail caused by alternating centrifugal force and a natural high-frequency blade vibration (Fig. 1). For example, observations of service-exposed Ti-based alloy fan blade-disk couples in fan engine propulsion systems revealed the presence of severe fretting fatigue damage on the contacting surfaces of blade dovetails and disk slots [10].

The objective of this investigation is to study and evaluate the extent of fretting damage on γ-TiAl (Ti-48Al-2Cr-2Nb in atomic percent) in contact with nickel-base superalloy at temperatures from 296 to 823 K. Reference experiments were also conducted with Ti-6Al-4V. Since the controlling operating parameters in common fretting, which are the specifics of the microscopic surface-parallel motion, such as frequency, amplitude and load, are not completely identified, these parameters are examined in this study. Vertically scanning interference microscopy (non-contact optical profilometry) was used to evaluate surface characteristics, such as surface topography, surface roughness, material transfer, and wear volume loss. Scanning electron microscopy (SEM) with energy dispersive spectroscopy (EDS) is used to determine the morphology and elemental composition of fretted surfaces, material transfer, and wear debris.

## 2. Materials

The Ti-48Al-2Nb-2Cr specimens were determined to be of the following composition (in at.%): titanium, 47.9; aluminum, 48.0; niobium, 1.96; chromium, 1.94; carbon, 0.013; nitrogen, 0.014; and oxygen, 0.167. The tensile properties are shown in Table 1. Note that the ultimate tensile strength of superalloy is greater than that of Ti-48Al-2Nb-2Cr by a factor of ~3.5 at room temperature and ~2 at high temperature (~1000 K).

The reference Ti-6Al-4V specimens examined were of the following nominal composition (in wt.%): titanium, balance; aluminum, 5.5-6.75; vanadium, 3.5-4.5; iron, ≤0.30; carbon, ≤0.08; nitrogen, ≤0.05; oxygen, ≤0.20; and hydrogen, ≤0.015 [15].

## 3. Experiments

Figure 2 presents the fretting wear apparatus used in the investigation. Fretting wear experiments were conducted with 9.4-mm diameter hemispherical nickel-base superalloy pins in contact with Ti-48Al-2Cr-2Nb flats or with 6-mm-diameter, hemispherical Ti-48Al-2Cr-2Nb pins in contact with nickel-base superalloy flats in air at temperatures from 296 to 823 K. All the flat and pin specimens used were polished with 3-μm-diameter diamond powder. Both pin and flat surfaces were relatively smooth, having centerline-average roughness $R_a$ in the range from 18 to 83 nm (Table 2). The Vickers hardness, measured at a load of 1.0 N, for the polished flat and pin specimens is also shown in Table 2.

All fretting wear experiments were conducted at loads from 1.0 N to 40 N, frequencies of 50, 80, 120, and 160 Hz, and slip amplitudes between 50 to 200 μm for 1 million to 20 million cycles. Both pin and flat surfaces were rinsed with 200-proof ethyl alcohol before installation in the fretting apparatus.

Two or three fretting experiments were conducted with each material couple at each fretting condition. The data were averaged to obtain the wear volume losses of Ti-48Al-2Cr-2Nb. The wear volume loss was determined by using an optical profiler (noncontact, vertical scanning, white-light interference microscope). It characterizes and quantifies surface roughness, height distribution, and critical dimensions (such as area and volume of damage, wear scars, and topographical features). It has three-dimensional profiling capability with excellent precision and accuracy (e.g., profile heights ranging from ≤1 nm up to 5 mm with 0.1-nm height resolution). The shape of a surface can be displayed by a computer-generated map developed from digital data derived from a three-dimensional interferogram of the surface. A computer directly processes the quantitative volume and depth of a fretted wear scar. Reference fretting wear experiments were conducted with 9.4-mm diameter hemispherical Ti-6Al-4V pins in contact with nickel-base superalloy flats.

## 4. Results and Discussion

### 4.1. Adhesion and Material Transfer

The surfaces of a titanium-base alloy and a superalloy resulted in a very strong interfacial adhesion (solid state or cold welding) when two such materials were brought into contact under fretting. For example, Fig. 3 presents a SEM backscattered electron image and an EDS spectrum taken from the fretted surface of the nickel-base superalloy pin after contact with the Ti-48Al-2Cr-2Nb flat. Clearly, Ti-48Al-2Cr-2Nb transferred to superalloy. The adhesive bonds formed at the interface of Ti-48Al-2Cr-2Nb and superalloy were sufficiently strong so that the cohesive bonds in the Ti-48Al-2Cr-2Nb were fractured because the ultimate tensile strength of superalloy is greater than that of Ti-48Al-2Nb-2Cr by a factor of ~3.5 at room temperature and ~2 at high temperature (~1000 K). The Ti-48Al-2Cr-2Nb failed either in tear or in shear. The failed Ti-48Al-2Cr-2Nb subsequently transferred to the superalloy surface. Progressive fretting produced scuffing or galling (localized damage). The amounts of the transferred Ti-48Al-2Cr-2Nb ranged from 10 to 60 percent of the superalloy contact area at all fretting conditions in this study. The thickness of the transferred Ti-48Al-2Nb-2Cr ranged up to ~20 μm. Figure 4, as an example, shows optical interferometry images, three-dimensional overview and front view, taken from the damaged surface of a nickel-base superalloy pin after contact with the Ti-48Al-2Cr-2Nb flat under fretting. Clearly the surface damage consisted of deposited Ti-48Al-2Cr-2Nb (material transfer), pits, grooves, fretting craters, and plastic deformation. The critical dimensions (area and thickness) of transferred material were characterized and quantified from such optical interferometry images.

As with the materials pair of Ti-48Al-2Cr-2Nb and superalloy, material transfer was observed on the superalloy flat surface after fretting against the Ti-6Al-4V pin in air at 296, 696 and 823 K. However, the degree of Ti-6Al-4V transfer was remarkably different and greater, ranging from 30 to 100 percent of the superalloy contact area for identical fretting conditions. The thickness ranged up to 50 μm.

4.2. Wear Behavior of Ti-48Al-2Cr-2Nb

Figure 5 shows typical wear scars produced on the Ti-48Al-2Cr-2Nb pin and the superalloy flat with fretting. Because of the specimen geometry a large amount of wear debris was deposited just outside the circular contact area. Pieces of the metal (both Ti-48Al-2Cr-2Nb and superalloy) and their oxides were torn out during fretting. It appears that the cohesive bonds in some of the contacting area of both metals fractured. SEM and EDS studies of wear debris produced under fretting verified the presence of metallic particles of both Ti-48Al-2Cr-2Nb and superalloy. In the central region of wear scars produced on Ti-48Al-2Cr-2Nb there was generally a large, shallow pit, where the Ti-48Al-2Cr-2Nb had torn out or sheared off and subsequently transferred to superalloy. The central regions of wear scars produced on Ti-48Al-2Cr-2Nb and on superalloy were morphologically similar (Fig. 5), generally having wear debris, scratches, plastically deformed asperities, and cracks.

Figure 6 shows examples of surface damages: metallic wear debris of Ti-48Al-2Cr-2Nb and superalloy, oxides and their debris, scratches (grooves), craters, plastically deformed asperities, and cracks. The scratches (Fig. 6(a)) can be caused by hard protuberance (asperities) on the superalloy surface (two-body conditions) or by wear particle between the surfaces (three-body conditions). Abrasion is a severe form of wear. The hard asperities and trapped wear particles plow or cut the Ti-48Al-2Cr-2Nb surface. The trapped wear particles have a scratching effect on both surfaces. Figure 7 shows an example of large, deep grooves where the wear debris particles have scratched the Ti-48Al-2Cr-2Nb surface in the slip direction under fretting at a slip amplitude of 200 μm and a temperature of 296 K. The volume loss of this particular Ti-48Al-2Cr-2Nb wear scar calculated from the three-dimensional image was $4.8\times10^{6}$ $\mu m^{3}$.

Because the hard asperities and trapped wear particles carry part of the load, they cause concentrated pressure peaks on both surfaces. The pressure peaks may well be the origin of crack nucleation in the oxide layers and the bulk alloys. There are two types of cracks observed on the wear surface of Ti-48Al-2Cr-2Nb: cracks in oxide layers and cracks in bulk Ti-48Al-2Cr-2Nb.

Oxide layers readily form on the Ti-48Al-2Cr-2Nb surface at 823 K and are often a favorable solution to wear problems. However, if the bulk Ti-48Al-2Cr-2Nb is not hard enough to carry the load, it will deform plastically or elastically under fretting contact. With Ti-48Al-2Cr-2Nb, cracks occurred in the oxide layer both within and around the contact areas (Fig. 6(b)).

Fractures in the protective oxide layers produced cracks in the bulk Ti-48Al-2Cr-2Nb (Fig. 6(c)) and also produced wear debris; chemically active, fresh surfaces; plastic deformation; craters; and fracture pits (Fig. 6(d)). The wear debris caused third-body abrasive wear (Fig. 6(a)). Local, direct contacts between the fresh surfaces of Ti-48Al-2Cr-2Nb and superalloy resulted in increased adhesion and local stresses, which may cause plastic deformation, flake-like wear debris, craters, and fracture pits (e.g., fracture pits in the Ti-48Al-2Cr-2Nb shown in Fig. 6(d)).

Cross sections of a wear scar on Ti-48Al-2Cr-2Nb revealed subsurface cracking and craters. For example, Fig. 8 shows propagation of subsurface cracking, nucleation of small cracks, formation of a large crater, and generation of debris. Cracks are transgranular and have no preference to the microstructure.

### 4.3. Wear Behavior of Nickel-Base Superalloy

Figure 9 shows examples of surface damage produced on superalloy: metallic wear debris of superalloy and Ti-48Al-2Cr-2Nb, oxides, scratches (grooves), small craters, plastically deformed asperities, and cracks, all of which are similar to those observed on Ti-48Al-2Cr-2Nb. The scratches (Fig. 9 (a)) can be caused by hard, oxidized wear particles of superalloy and Ti-48Al-2Cr-2Nb, which are trapped between the interacting surfaces or are adhered to or embedded in the counterpart Ti-48Al-2Cr-2Nb surface. In Fig. 9 (a) scratches, craters, and fracture pits were produced by abrasion, a severe form of wear. The trapped wear particles and the adhered (or embedded) wear particles plow or cut the superalloy surface. The trapped wear particles have a scratching effect on both surfaces; and because they carry part of the load, they cause concentrated pressure peaks on both surfaces. The pressure peaks may well be the origin of crack nucleation in the oxide layers and the bulk alloys.

Oxide layers readily form on the superalloy surfaces at 823 K and are often a favorable solution to wear problems. However, cracks occurred in the oxide layers both within and around the contact areas, as shown in Fig. 9(b).

Fractures in the protective oxide layers produced cracks in the bulk superalloy (Fig. 9 (c)) and also produced wear debris, chemically active fresh surfaces, plastic deformation, craters, and fracture pits (Fig. 9(d)). This wear debris can cause third-body abrasive wear. Local, direct contacts between the fresh surfaces of Ti-48Al-2Cr-2Nb and superalloy resulted in increased adhesion and local stresses, which may cause plastic deformation, flakelike wear debris, craters, and fracture pits.

4.4. Parameters that Influence Wear Loss of Ti-48Al-2Cr-2Nb

Temperature influences the adhesion, deformation, and fracture behaviors of contacting materials in relative motion. It is known that temperature interacts with the fretting process in two ways: first, the rate of oxidation or corrosion increases with temperature; and second, the mechanical properties, such as hardness, of the materials are also temperature dependent [7]. Figure 10 presents the wear volume loss measured by optical interferometry as a function of temperature for Ti-48Al-2Cr-2Nb in contact with superalloy. Also, SEM images and EDS spectra were taken from the fretted Ti-48Al-2Cr-2Nb surfaces. The wear volume loss dropped to a low value at 473 K. The worn surface at 473 K was predominantly oxide and relatively smooth. A protective oxide film prevented direct metal-to-metal contact and ensured, in effect, that a mild oxidative wear regime prevailed. However, fretting wear increased as the temperature was increased from 473 to 823 K. The higher temperatures of 723 and 823 K resulted in oxide film disruption with crack generation, loose wear debris, and pitting of the Ti-48Al-2Cr-2Nb wear surface.

Figure 11 shows the wear volume loss measured by the optical interferometer as a function of fretting frequency for Ti-48Al-2Cr-2Nb in contact with superalloy at different temperatures of 296 and 823 K, at a load of 30 N, with constant slip amplitude of 50 μm, and for a constant fretting duration of 1 million cycles.

The results indicate that fretting frequencies influence the volume loss of Ti-48Al-2Cr-2Nb. Although there were some exceptions, the wear volume loss generally decreased with increasing fretting frequency. A reasonable amount of material transfer from the Ti-48Al-2Cr-2Nb specimen to the superalloy specimen was observed at all frequencies. At lowest frequency of 50 Hz remarkable plastic deformation (grooving) and surface roughing in the Ti-48Al-2Cr-2Nb wear scar were observed. At high frequencies wear scars were noticeably smooth with bulk cracks in the Ti-48Al-2Cr-2Nb surface.

Figure 12 shows the wear volume loss measured by optical interferometry as a function of slip amplitude for Ti-48Al-2Cr-2Nb in contact with superalloy. The fretting wear volume loss increased as the slip amplitude increased. Increases in slip amplitude tend to produce more metallic wear debris, causing severe abrasive wear in the contacting metals.

Figure 13 shows the wear volume loss as a function of load for Ti-48Al-2Cr-2Nb in contact with superalloy at a temperature of 823 K, a fretting frequency of 80 Hz, and a slip amplitude of 50 μm for 1 million cycles. The fretting wear volume loss generally increased as the load increased, generating more metallic wear debris in the contact area, the prime cause of the abrasive wear in both Ti-48Al-2Cr-2Nb and superalloy.

## 5. Summary and Concluding Remarks

The fretting wear behavior of γ-TiAl (Ti-48Al-2Cr-2Nb) in contact with a typical nickel-base superalloy in air at temperature of 296 to 823 K was examined with the following results:

1. The interfacial adhesive bonds between Ti-48Al-2Cr-2Nb and superalloy were generally stronger than the cohesive bonds within Ti-48Al-2Cr-2Nb. The failed Ti-48Al-2Cr-2Nb subsequently transferred to the superalloy and caused scuffing or galling.

2. Ti-6Al-4V transfer was observed on the superalloy as with the materials pair of Ti-48Al-2Cr-2Nb and superalloy. However, the degree of Ti-6Al-4V transfer was greater.

3. The wear scars produced on Ti-48Al-2Cr-2Nb contained metallic and oxide wear debris, scratches, plastically deformed asperities, cracks, and fracture pits.

4. The wear damage of superalloy was analogous to that of Ti-48Al-2Cr-2Nb. The wear scars produced on superalloy contained transferred Ti-48Al-2Cr-2Nb, metallic and oxide wear debris, scratches, plastically deformed asperities, cracks, and fracture pits.

5. The oxidation rate of Ti-48Al-2Cr-2Nb generally increased with increasing temperature. Although oxide layers readily formed on the Ti-48Al-2Cr-2Nb surface at all temperatures, cracking readily occurred in the oxide layers both within and around the contact areas.

6. Compared with the wear volume loss of Ti-48Al-2Cr-2Nb at 296 K, it dropped to a lower value at 473 K, that is, the increasing rate of oxidation at elevated temperatures to 473 K led to the drop in wear volume loss. Mild oxidative wear was observed at 473 K. However, the wear volume loss increased with increasing temperature in the range from 473 to 823 K. The higher temperatures of 723 and 823 resulted in oxide film disruption with crack generation, loose wear debris, and pitting of the Ti-48Al-2Cr-2Nb wear surface.

7. The wear volume loss of Ti-48Al-2Cr-2Nb generally decreased with increasing fretting frequency. However, it increased with increasing slip amplitude, and increased with increasing load. Both increasing slip amplitude and increasing load tended to produce more metallic wear debris, causing severe abrasive wear in the contacting metals.

**Acknowledgments**

This work was funded by the ULTRASAFE project with Ms. Susan M. Johnson as Project Manager.

The authors are grateful to Dr. Sai V. Raj (Sub-Project Team Leader), Dr. Gary R. Halford, and Dr. Michael V. Nathal for helpful discussions.

**References**

1. T.E. Tallian, Failure atlas for Hertz contact machine elements, Chapter 9 Fretting wear, ASME Press, New York (1992) pp. 141–154.
2. R.B. Waterhouse, Plastic deformation in fretting processes—a Review, in "Fretting Fatigue: current technology and practices," Eds. D.W. Hoeppner, V. Chandrasekaran, C.B. Elliot III, ASTM STP 1367, West Conshohocken, PA, (2000) pp. 3–18.
3. R.B. Waterhouse, Occurrence of fretting in practice and its simulation in the laboratory, in "Materials evaluation under fretting conditions," ASTM special Technical Publication 780, Philadelphia, PA (1982) pp. 3–16.29.
4. D. Kusner, C. Poon, and D.W. Hoeppner, A new machine for studying surface damage due to wear and fretting, in "Materials evaluation under fretting conditions," ASTM special Technical Publication 780, Philadelphia, PA (1982) pp. 3–16.
5. T. Satoh, Influence of microstructure on fretting fatigue behavior of a near-alpha titanium, in "Fretting Fatigue: current technology and practices," Eds. D.W. Hoeppner, V. Chandrasekaran, C.B. Elliot III, ASTM STP 1367, West Conshohocken, PA, (2000) pp. 295–307.
6. C. Lutynski, G. Simansky, and A.J. McEvily, Fretting fatigue of Ti-6Al-4V alloy, in "Materials evaluation under fretting conditions," ASTM special Technical Publication 780, Philadelphia, PA (1982) pp. 150–164.
7. R.C. Bill, Review of factors that influence fretting wear, in "Materials evaluation under fretting conditions," ASTM special Technical Publication 780, Philadelphia, PA (1982) pp. 165–182.

8. T. Hansson, M. Kamaraj, Y. Mutoh, and B. Pettersson, High temperature fretting fatigue behavior in an XD γ-base TiAl, in "Fretting Fatigue: current technology and practices," eds. D.W. Hoeppner, V. Chandrasekaran, C.B. Elliot III, ASTM STP 1367, West Conshohocken, PA, (2000) pp. 65–79.
9. R.H. VanStone, B.H. Lawless, and M. Hartle, Fretting in Ti-6Al-4V at room temperature, in Proceedings of 5th National Turbine Engine High Cycle Fatigue (HCF) Conference, 7–9 March 2000, Sheraton San Marcos Hotel, chandler, Arizona (2000).
10. S. Chakravarty, R.G. Andrews, P.C. Patnaik, and A.K. Koul, The effect of surface modification on fretting fatigue in Ti alloy turbine components, JOM (1995) pp. 31–35.
11. D. Hoeppner, S. Adibnazari, and M.W. Moesser, Literature review and preliminary studies of fretting and fretting fatigue including special applications to aircraft joints, Report No. DOT/FAA/CT–93/2, Defense Technical Information Center, Ft. Belvoir, VA (1994).
12. A.L. Hutson and T. Nicholas, Fretting fatigue behavior of Ti-6Al-4V against Ti-6Al-4V under flat-on-flat contact with blending radii, in "Fretting Fatigue: current technology and practices," Eds. D.W. Hoeppner, V. Chandrasekaran, C.B. Elliot III, ASTM STP 1367, West Conshohocken, PA, (2000) pp. 308–321.
13. D.W. Hoeppner, V. Chandrasekaran, and C.B. Elliott III (editors), Fretting Fatigue: Current Technology and Practices, ASTM STP 1367, West Conshohocken, PA 19428–2959, 2000.
14. S.R. Brown (Symposium Chairman), Materials Evaluation Under Fretting Conditions, ASTM 780, Philadelphia, PA 19103, 1982.
15. Donachie, M.J. (Ed.) Titanium and Titanium Alloys, Source Book, American Society for Metals, Metals Park, OH, 1982.

Table 1.—Tensile Properties of Ti-48Al-2Cr-2Nb

| Temperature, K | Modulus, GPa | Ultimate Tensile Strength, MPa |
|---|---|---|
| 293 | 170 | 410 |
| 923 | 140 | 460 |

Table 2.—Surface Roughness and Vickers Hardness of Specimens

| Specimen | Average roughness, $R_a$, nm | | Hardness, $H_v$ (load, 1 N), GPa | |
|---|---|---|---|---|
| | Mean | Standard deviation | Mean | Standard deviation |
| Ti-48Al-2Cr-2Nb pin | 42 | 7.1 | 4.12 | 0.42 |
| Nickel-base superalloy pin | 40 | 8.9 | 5.52 | 0.44 |
| Ti-6Al-4V pin | 83 | 2.0 | 3.85 | 0.092 |
| Ti-48Al-2Cr-2Nb flat | 35 | 3.3 | 3.78 | 0.57 |
| Nickel-base superalloy flat | 18 | 7.2 | 4.78 | 0.21 |

Fig. 7 Optical interferometry three-dimensional image of damaged surface of Ti-48Al-2Cr-2Nb flat fretted against nickel-base superalloy pin, showing severe abrasive wear. Fretting conditions: load, 30 N; frequency, 50 Hz; slip amplitude, 200 μm; number of fretting cycles, 1 million; environment, air; and temperature, 296 K.

Fig. 8 Cross-section view of wear scar on Ti-48Al-2Cr-2Nb flat in contact with superalloy pin. (a) Overview. (b) Crack growth. Fretting conditions: load, 30 N; frequency, 80 Hz; slip amplitude, 70 μm; number of fretting cycles, 20 million; environment, air; and temperature, 823 K.

Fig. 9 Surface and subsurface damage in superalloy pin in contact with Ti-48Al-2Cr-2Nb flat. (a) Scratches. (b) Cracks in oxide layers. (c) Cracks in metal. (d) Fracture pits and plastic deformation. Fretting conditions: load, 1 N; frequency, 80 Hz; slip amplitude, 50 μm; number of fretting cycles, 1 million; environment, air; and temperature, 823 K.

Fig. 10 Wear volume loss of Ti-48Al-2Cr-2Nb flat in contact with superalloy pin as function of fretting temperature. Fretting conditions: load, 30 N; fretting frequencies, 50, 80, 120, and 160 Hz; slip amplitude, 50 μm; number of fretting cycles, 1 million; and environment, air.

Fig. 11 Wear volume loss of Ti-48Al-2Cr-2Nb flat in contact with superalloy pin as function of fretting frequency. Fretting conditions: load, 30 N; slip amplitude, 50 μm; number of fretting cycles, 1 million; environment, air; and temperature, 823 K. 296 and

Fig. 12 Wear volume loss of Ti-48Al-2Cr-2Nb flat in contact with superalloy pin as function of slip amplitude. Fretting conditions: load, 30 N; frequency, 50 Hz; number of fretting cycles, 1 million; environment, air; and temperatures, 296 and 823 K.

**Figure Legends**

Fig. 1 Fan and compressor blade dovetail displacements

Fig. 2 Fretting apparatus

Fig. 3 Wear scar on nickel-base superalloy pin fretted against Ti-48Al-2Cr-2Nb flat. (a) SEM backscattered electron image. (b) X-ray energy spectrum with EDS. Fretting conditions: load, 1.5 N; frequency, 80 Hz; slip amplitude, 50 μm; number of fretting cycles, 1 million; environment, air; and temperature, 823 K.

Fig. 4 Optical interferometry images of damaged surface of nickel-base superalloy pin fretted against Ti-48Al-2Cr-2Nb flat. (a) Three-dimensional view. (b) Side view. Volume of material transferred, $1.35\times10^5$ $\mu m^3$. Fretting conditions: load, 30 N; frequency, 50 Hz; slip amplitude, 150 μm; number of fretting cycles, 1 million; environment, air; and temperature, 823 K.

Fig. 5 Wear scars (a) on Ti-48Al-2Cr-2Nb pin and (b) on superalloy flat. Fretting conditions: load, 1 N; frequency, 80 Hz; slip amplitude, 50 μm; number of fretting cycles, 1 million; environment, air; and temperature, 823 K.

Fig. 6 Surface and subsurface damage in Ti-48Al-2Cr-2Nb flat in contact with superalloy pin. (a) Scratches. (b) Cracks in oxide layers. (c) Cracks in metal. (d) Fracture pits and plastic deformation. Fretting conditions: load, 1 N; frequency, 80 Hz; slip amplitude and number of fretting cycles, (a) 50 μm and 1 million, (b) 60 μm and 10 million, (c) 50 μm and 1 million, (d) 70 μm and 20 million; environment, air; and temperature, 823 K.

Fig. 7 Optical interferometry three-dimensional image of damaged surface of Ti-48Al-2Cr-2Nb flat fretted against nickel-base superalloy pin, showing severe abrasive wear. Fretting conditions: load, 30 N; frequency, 50 Hz; slip amplitude, 200 μm; number of fretting cycles, 1 million; environment, air; and temperature, 296 K.

Fig. 8 Cross-section view of wear scar on Ti-48Al-2Cr-2Nb flat in contact with superalloy pin. (a) Overview. (b) Crack growth. Fretting conditions: load, 30 N; frequency, 80 Hz; slip amplitude, 70 μm; number of fretting cycles, 20 million; environment, air; and temperature, 823 K.

Fig. 9 Surface and subsurface damage in superalloy pin in contact with Ti-48Al-2Cr-2Nb flat. (a) Scratches. (b) Cracks in oxide layers. (c) Cracks in metal. (d) Fracture pits and plastic deformation. Fretting conditions: load, 1 N; frequency, 80 Hz; slip amplitude, 50 μm; number of fretting cycles, 1 million; environment, air; and temperature, 823 K.

Fig. 10 Wear volume loss of Ti-48Al-2Cr-2Nb flat in contact with superalloy pin as function of fretting temperature. Fretting conditions: load, 30 N; fretting frequencies, 50, 80, 120, and 160 Hz; slip amplitude, 50 μm; number of fretting cycles, 1 million; and environment, air.

Fig. 11 Wear volume loss of Ti-48Al-2Cr-2Nb flat in contact with superalloy pin as function of fretting frequency. Fretting conditions: load, 30 N; slip amplitude, 50 μm; number of fretting cycles, 1 million; environment, air; and temperature, 296 and 823 K.

Fig. 12 Wear volume loss of Ti-48Al-2Cr-2Nb flat in contact with superalloy pin as function of slip amplitude. Fretting conditions: load, 30 N; frequency, 50 Hz; number of fretting cycles, 1 million; environment, air; and temperatures, 296 and 823 K.

Fig. 13 Wear volume loss of Ti-48Al-2Cr-2Nb flat in contact with superalloy pin as function of load. Fretting conditions: frequency, 80 Hz; slip amplitude, 50 μm; number of fretting cycles, 1 million; environment, air; and temperature, 823 K.

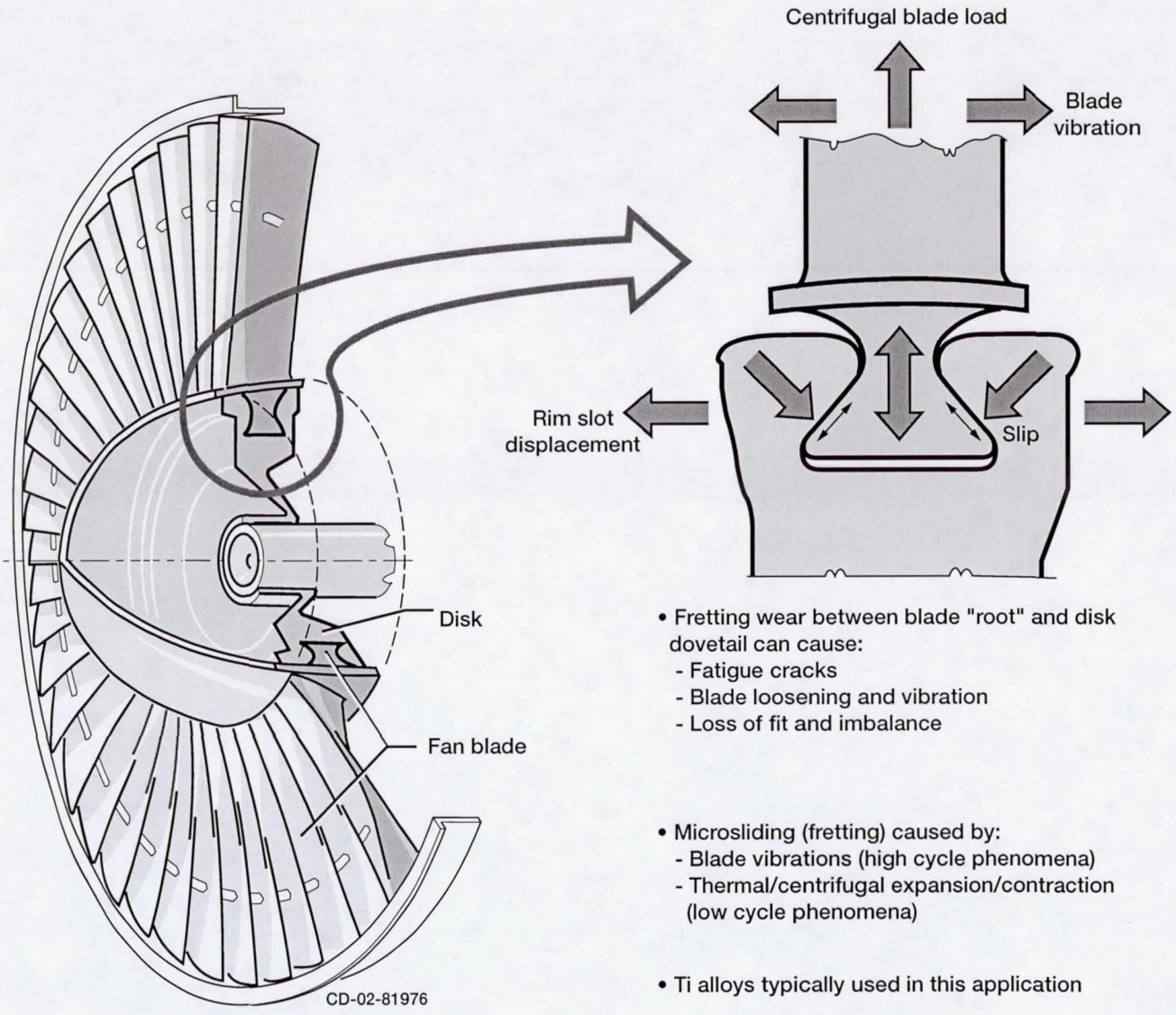


- Fretting wear between blade "root" and disk dovetail can cause:
  - Fatigue cracks
  - Blade loosening and vibration
  - Loss of fit and imbalance

- Microsliding (fretting) caused by:
  - Blade vibrations (high cycle phenomena)
  - Thermal/centrifugal expansion/contraction (low cycle phenomena)

- Ti alloys typically used in this application

Figure 1

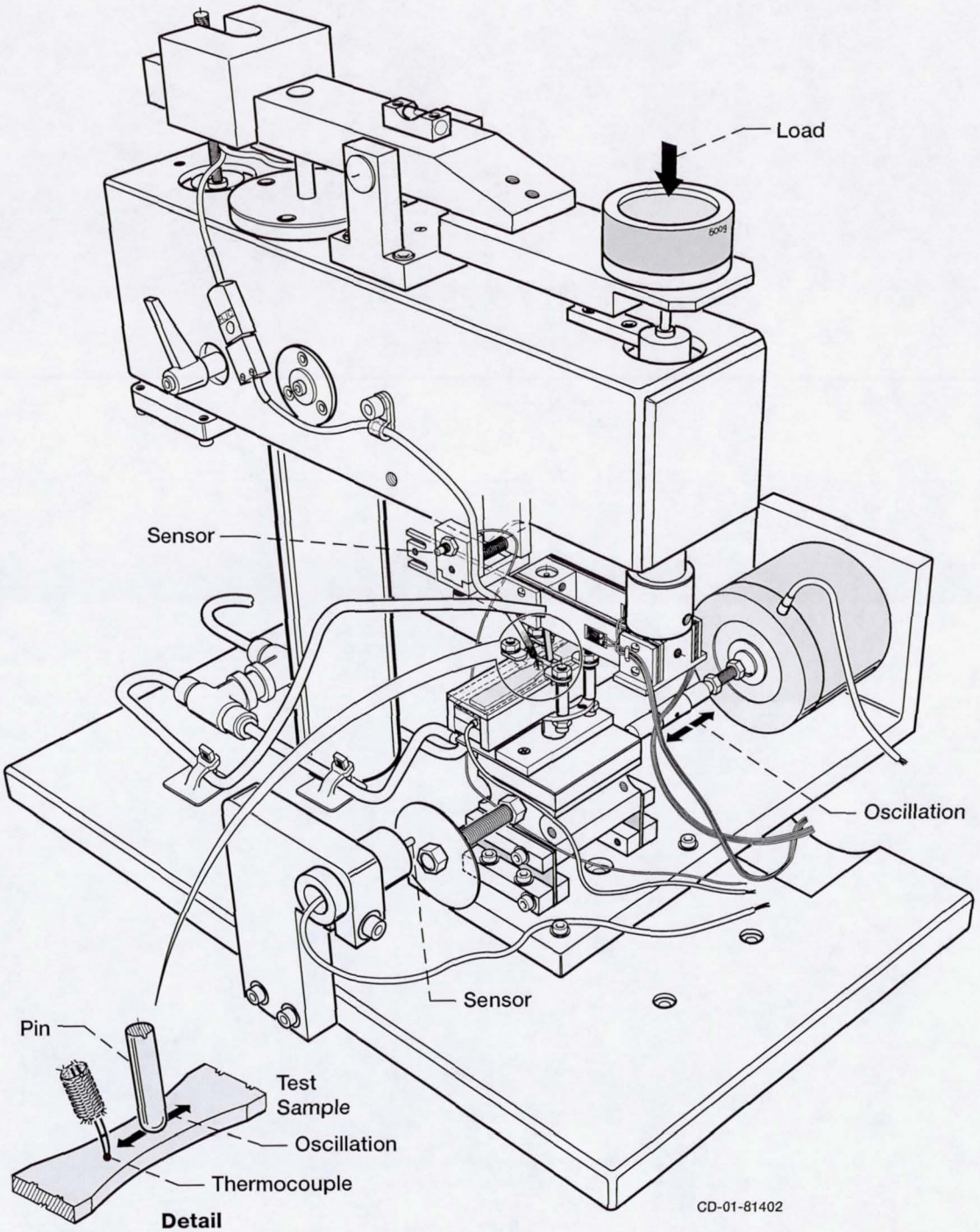
Load
Sensor
Oscillation
Sensor
Pin
Test
Sample
Oscillation
Thermocouple
Detail
CD-01-81402

Figure 2

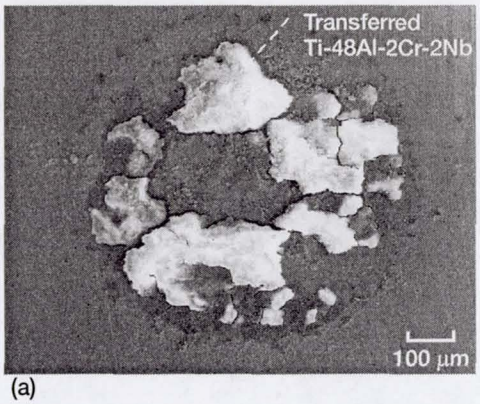
Transferred
Ti-48Al-2Cr-2Nb
100 μm

(a)

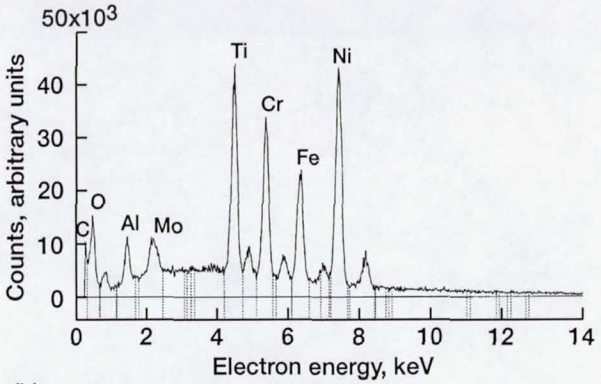
50x10^3
Counts, arbitrary units
40
30
20
10
0
C
O
Al
Mo
Ti
Cr
Fe
Ni
0
2
4
6
8
10
12
14
Electron energy, keV

(b)

Figure 3

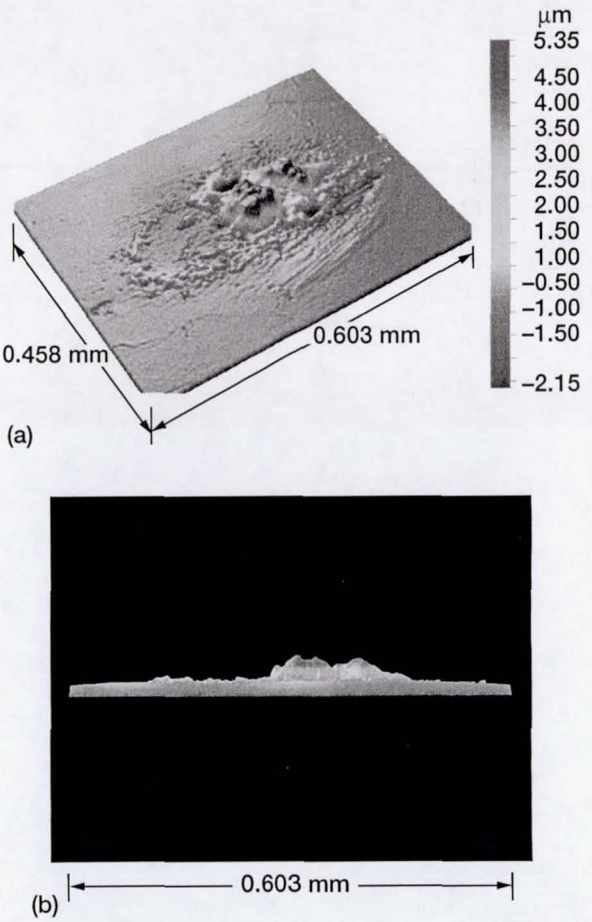
μm
5.35
4.50
4.00
3.50
3.00
2.50
2.00
1.50
1.00
−0.50
−1.00
−1.50
−2.15
0.458 mm
0.603 mm
(a)
0.603 mm
(b)

Figure 4

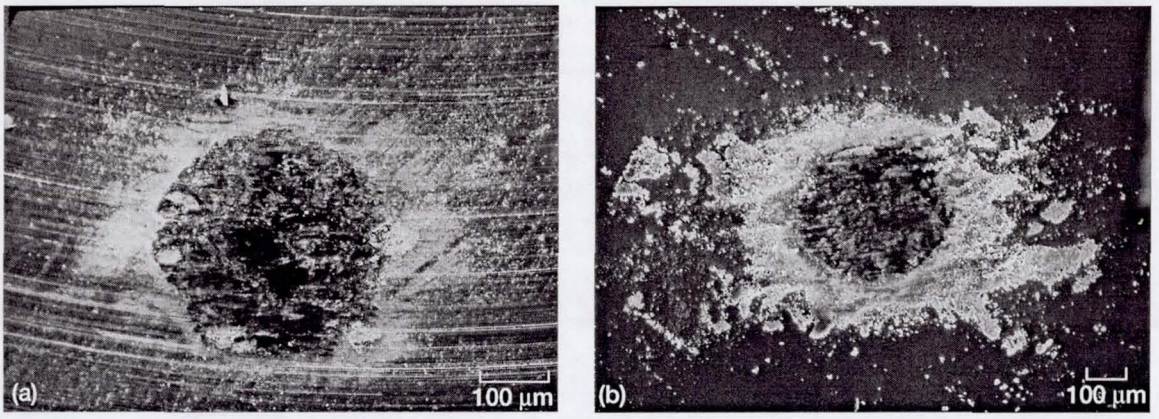


Figure 5

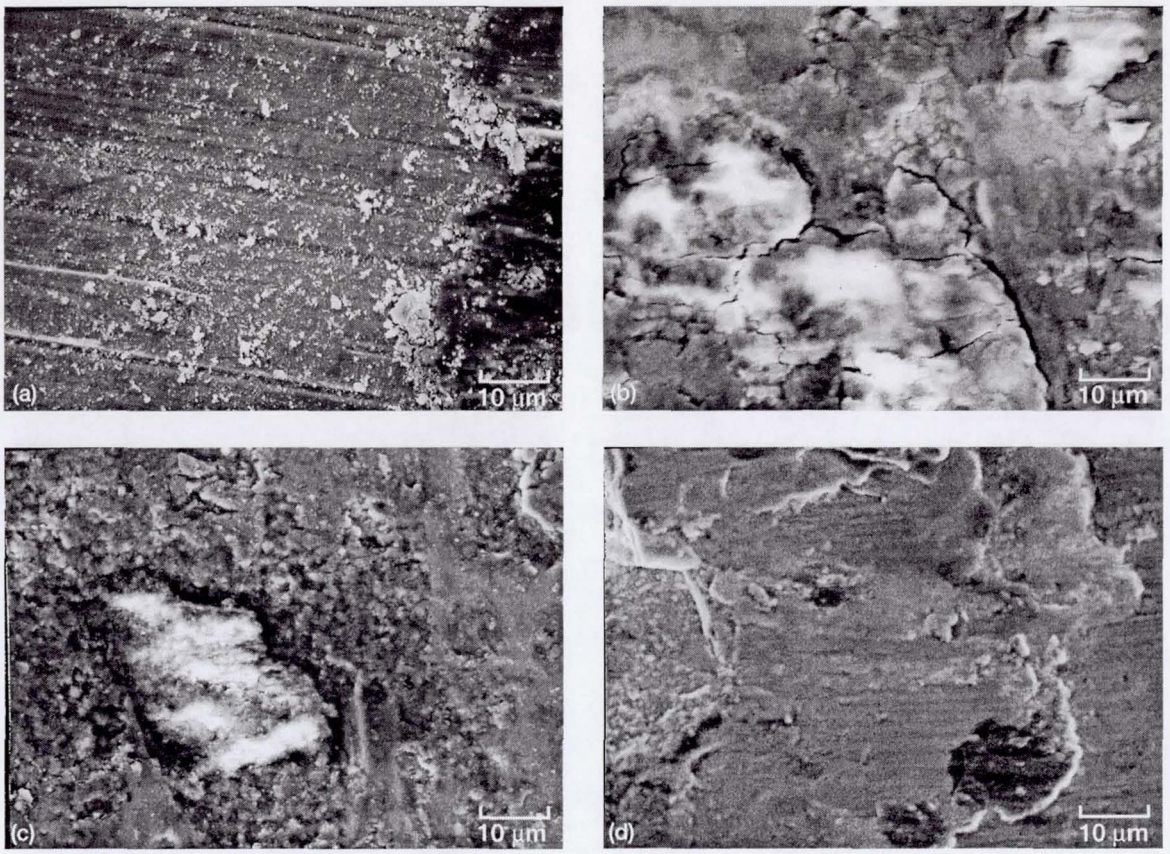


Figure 6

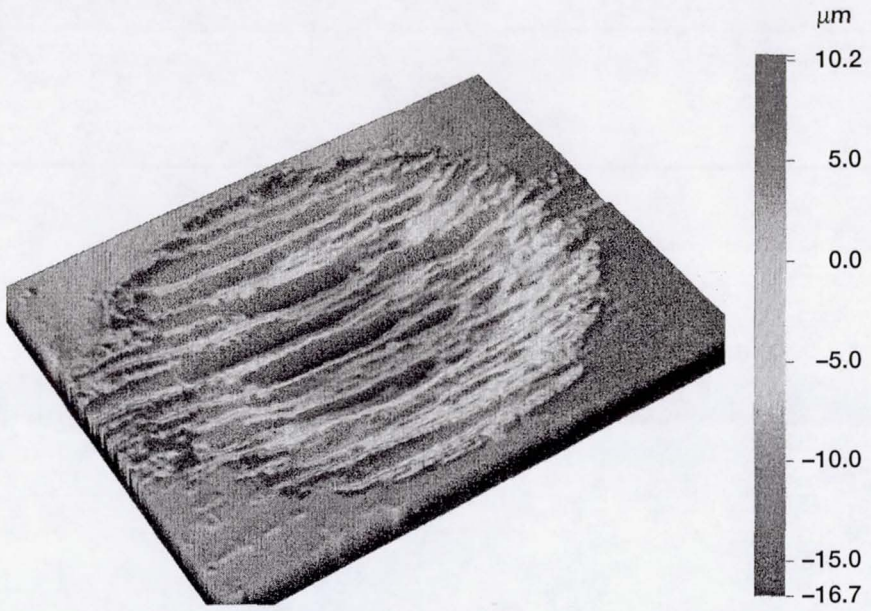


Figure 7

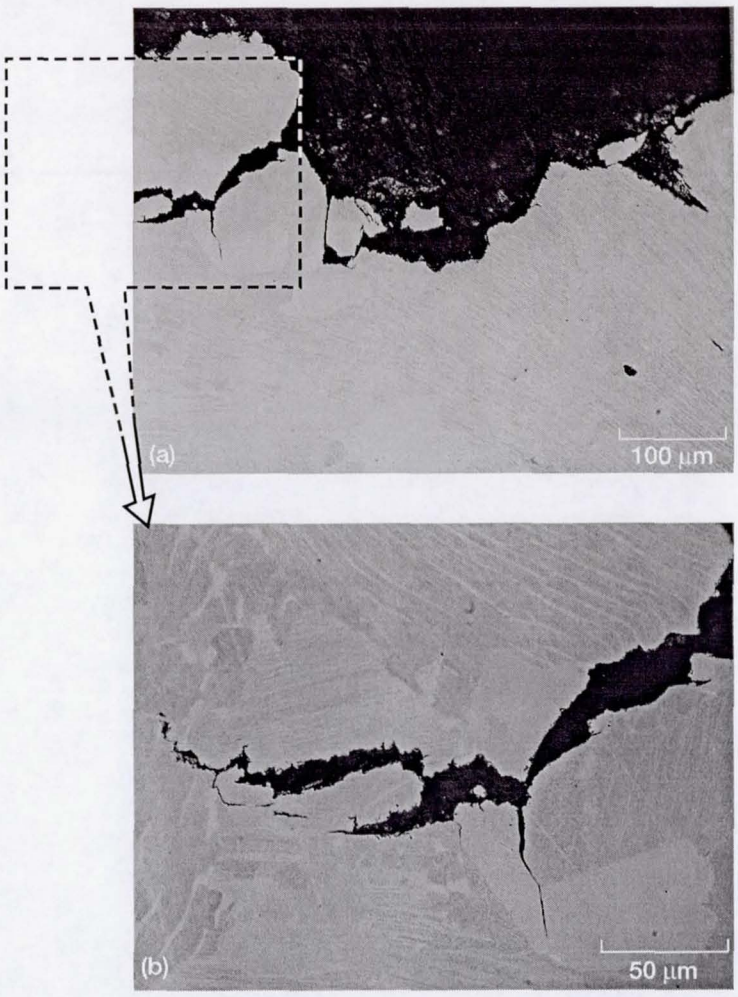


Figure 8

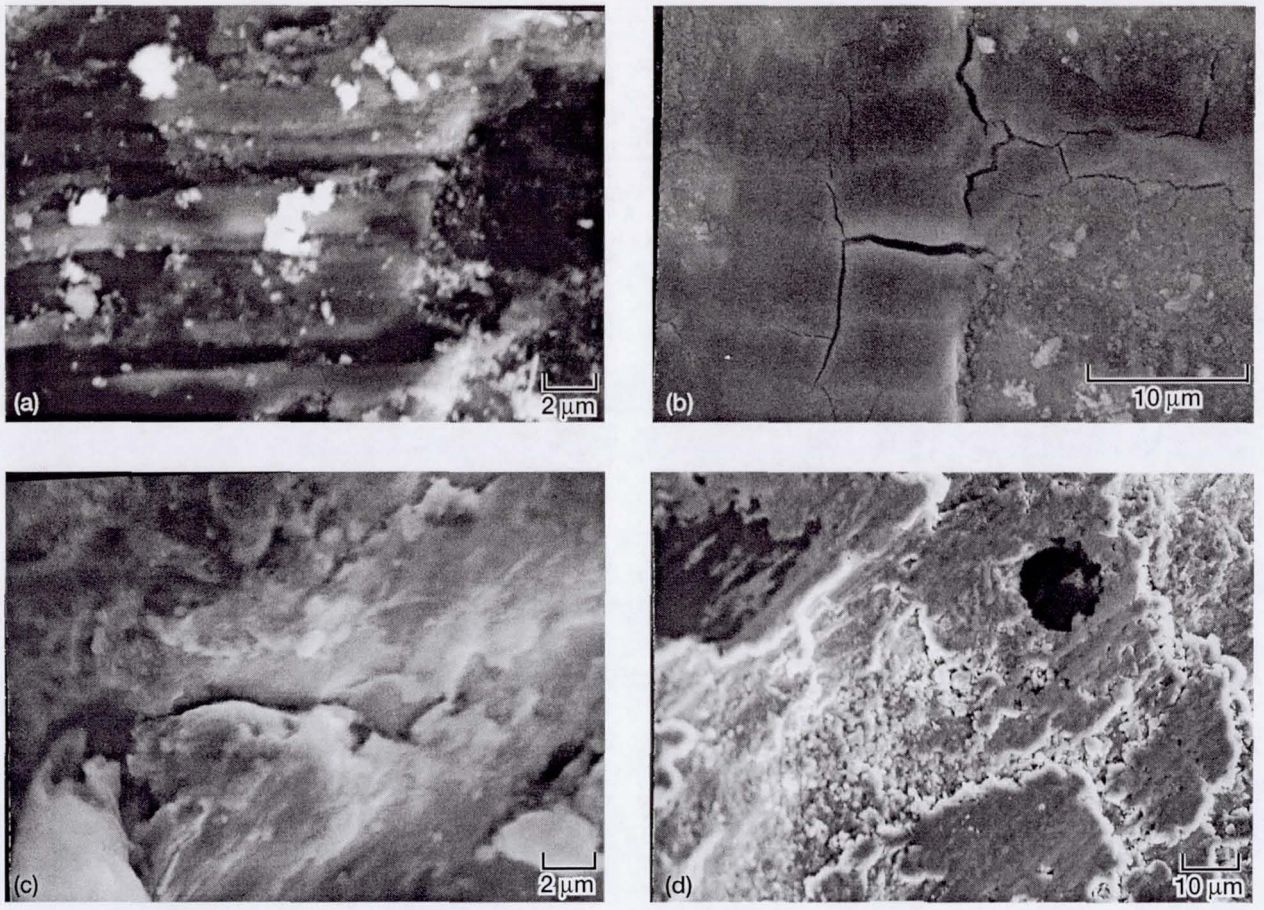


Figure 9

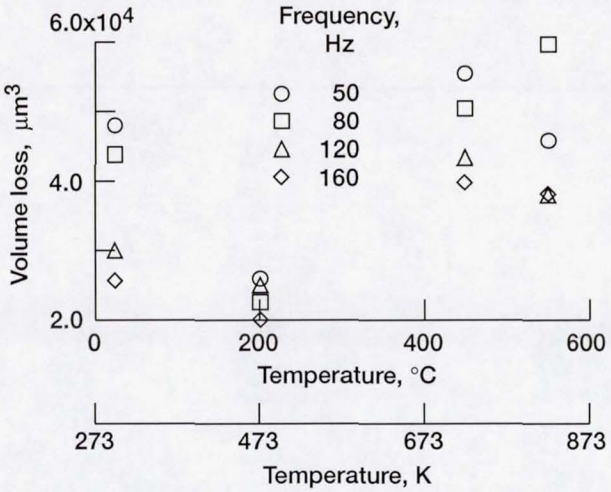
6.0x10^4
4.0
2.0
Volume loss, μm^3
Frequency, Hz
50
80
120
160
0
200
400
600
Temperature, °C
273
473
673
873
Temperature, K

Figure 10

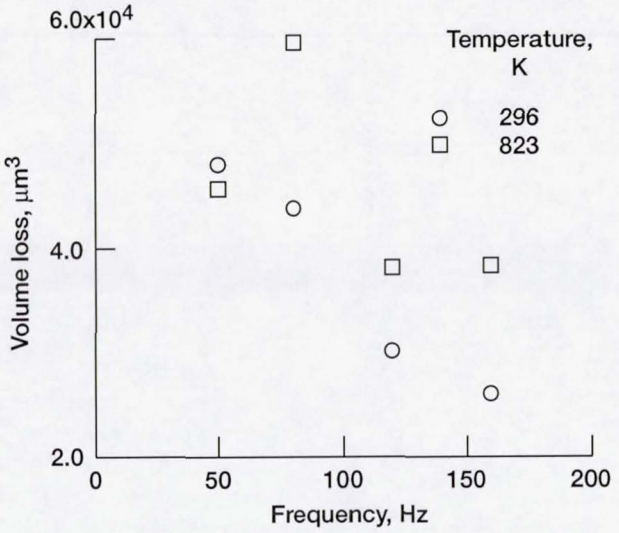
6.0x10^4
4.0
2.0
Volume loss, μm^3
0
50
100
150
200
Frequency, Hz
Temperature, K
296
823

Figure 11

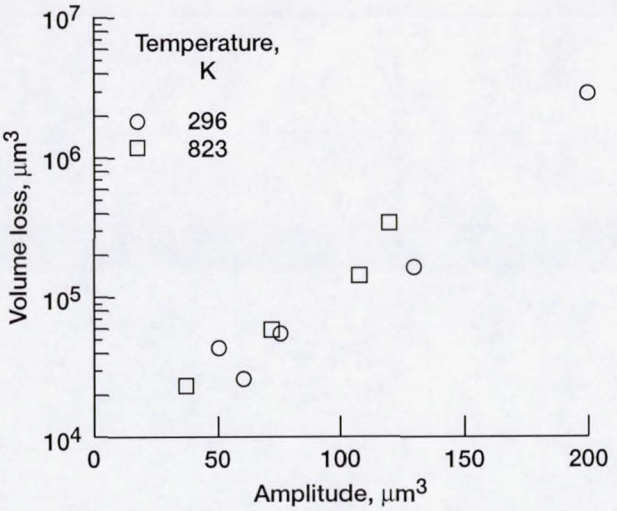
Temperature,
K
296
823
Volume loss, μm3
Amplitude, μm3
10^7
10^6
10^5
10^4
0
50
100
150
200

Figure 12

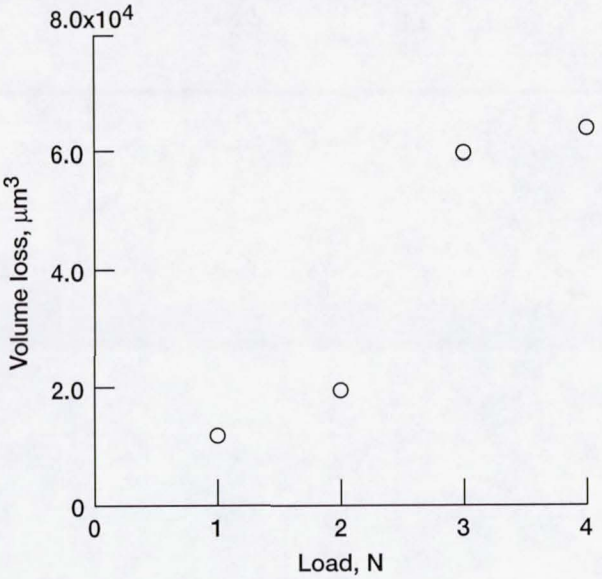


Figure 13